SUPPLEMENTAL MATERIAL

Dosage-sensitive functions in embryonic development drove the survival of genes on sex-specific chromosomes in snakes, birds, and mammals

Daniel W. Bellott and David C. Page

SUPPLEMENTAL METHODS

Reconstructing the ancestral autosomes

Ancestral sex-linked genes in caenophidian snakes

We downloaded peptide sequences and lists of human, chicken, and lizard orthologs from Ensembl (release 96)(Yates et al. 2019). To identify snake orthologs, we aligned these peptides to the reference genome assemblies of prairie rattlesnake (Schield et al. 2019), mainland tiger snake five-pacer, (Yin et al. 2016), and *Boa constrictor* (Bradnam et al. 2013), using blat (Kent 2002) in tblatx mode (-t=dnax –q=prot), and retained only the best hit for each peptide sequence (Table 1, Supplemental Table S1).

We seeded our search for the ancestral set of sex-linked genes with 106 genes previously mapped to the Z or W Chromosomes of caenophidian snakes (Matsubara et al. 2012, 2016; Vicoso et al. 2013a; Rovatsos et al. 2015; Yin et al. 2016; Perry et al. 2018) and the orthologous python Y Chromosome (Gamble et al. 2017) (Supplemental Table S2). Most of these genes have orthologs on human Chromosomes 3, 7, 10, 17, and 19; chicken Chromosomes 2 and 27; and lizard Chromosome 6.

We identified genes as sex-linked in the ancestor of caenophidian snakes by looking for orthologs of human, chicken, and lizard genes that were syntenic with published sex-linked genes in one or more of the three caenophidian snake genome assemblies, starting with prairie rattlesnake (the most contiguous). We used orthologous scaffolds in the *Boa constrictor* assembly as an outgroup to resolve whether lineage-specific gains and losses occurred before or after the divergence of henophidian and caenophidian snakes.

We found that 99 of 106 published snake sex-linked genes mapped to the prairie rattlesnake Z Chromosome assembly (CM012323.1). Of the seven remaining genes, five (*ARF1*, *KLF6*, *MRPL3*, *MYO1D*, and *ZBTB47*) mapped to autosomes in prairie rattlesnake, but were found on scaffolds syntenic with other Z-linked genes in tiger snake and five-pacer viper, and on autosomes orthologous to the Z Chromosome in outgroup species. The other two (*PINX1*, *TMEM35B*) are not syntenic with caenophidian Z-linked genes or their orthologs in any species, and probably represent genes acquired by the python Y Chromosome (Supplemental Table S3).

We identified 1648 genes as ancestral to the caenophidian sex chromosomes, including 1495 genes from the prairie rattlesnake Z Chromosome assembly, and 153 others based on synteny in other species (Supplemental Table S3). This set of ancestral genes includes 80 published W-linked genes from 13 caenophidian snake species (Matsubara et al. 2006, 2016; Vicoso et al. 2013a; Yin et al. 2016; Perry et al. 2018)(Supplemental Table S3). We also identified another 41 genes among our ancestral set that were previously identified as candidate W-linked genes in pygmy

rattlesnake and mountain garter snake (Vicoso et al. 2013a), but were rejected because their lizard orthologs did not map to lizard Chromosome 6 (Supplemental Table S5).

Our ancestral set of genes contains 348 members of 8 multi-copy gene families, including 18 of 41 candidate W-linked genes (Supplemental Table S3). Several of these gene families, particularly the olfactory receptor, vomeronasal receptor, and immunoglobulin heavy chain variable region families, form megabase-sized arrays that likely vary in copy-number between species. We excluded genes from 8 multi-copy families and restricted our analyses to single-copy genes where we could confidently assign orthologs across species, yielding a set of 1300 ancestral genes (Supplemental Table S3).

Pseudoautosomal boundaries

We used the published boundary of the pseudoautosomal region for five-pacer viper (Schield et al. 2019). To locate the pseudoautosomal boundaries in pygmy rattlesnake and mountain garter snake, we mapped male and female reads of pygmy rattlesnake (Vicoso et al. 2013a) to the prairie rattlesnake genome, and male and female reads from mountain garter snake (Vicoso et al. 2013a) to the eastern garter snake genome (*Thamnophis sirtalis*)(Perry et al. 2018) using bowtie2 (version 2.3.4.1)(Langmead et al. 2009) (Supplemental Table S1). We aligned the eastern garter snake genome with the prairie rattlesnake genome using LAST (version 992)(Kielbasa et al. 2011) to generate a chain file, which we filtered with `chainSort`, `chainNet`, and `netChainSubset` from the UCSC genome browser tools (version 0.0.3-1)(Haeussler et al. 2019). We converted read alignments into a coverage bedGraph using bedtools (version 2.26.0)(Quinlan and Hall 2010), and then used `liftOver` from the UCSC genome browser tools to map coordinates from eastern garter snake to the more contiguous prairie rattlesnake assembly. We plotted the base 2 logarithm of the ratio of normalized female to normalized male coverage across the Z Chromosome in 100 kilobase windows, to visualize the transition from equal read depth in both sexes in the pseudoautosomal region to lower coverage in females in the younger evolutionary strata on the Z Chromosome (Supplemental Figures S3 and S4). We note that read coverage in ancestral arrays of multicopy gene families was greater in mountain garter snake females than in males, but we cannot distinguish between extreme polymorphism in array size on the Z Chromosome between individuals, or expansion of these arrays on the W Chromosome.

Reconstructing evolutionary strata

Phylogenetic analyses

For cross-species phylogenetic analyses, we generated multiple alignments using Clustal Omega (version 1.2.4)(Sievers et al. 2011) and PAL2NAL (version 14)(Suyama et al. 2006) (Supplemental Data S2). For each alignment, we generated a set of phylogenetic trees based on the species trees from TimeTree (Kumar et al.

2017) (Supplemental Fig. S1), allowing for stratum formation events in the common ancestor, or in later lineages. We used TreePuzzle (version 5.2)(Schmidt et al. 2002) to estimate the gamma distribution parameter and transition-transversion ratio. We used TreePuzzle together with DNAML and DNAPARS in PHYLIP (version 3.696)(Felsenstein 1989) to evaluate which trees were most consistent with the multiple alignment, using the Shimodaira-Hasegawa test (Shimodaira and Hasegawa 1999).

Caenophidian evolutionary strata analyses

We seeded our search for homologs of ancestral ZW pairs with coding sequences of the longest isoforms of human, chicken, and lizard orthologs from Ensembl. To expand our temporal resolution in the caenophidian lineage, we used exonerate (version 2.2.0)(Slater and Birney 2005) to predict coding sequences from genomic reference sequences in *Boa constrictor (*Bradnam et al. 2013), Burmese python (*Python molurus bivittatus*) (Castoe et al. 2013), speckled rattlesnake (*Crotalus mitchellii*)(Gilbert et al. 2014), prairie rattlesnake (Schield et al. 2019), timber rattlesnake (*Crotalus horridus*) (Sanders, et al. Unpublished), Taiwan habu (*Protobothrops mucrosquamatus*)(Aird et al. 2017), Okinawa habu (*Protobothrops flavoviridis*) (Shibata et al. 2018), five-pacer viper, adder (*Vipera berus berus*) (Liu, et al. Unpublished), eastern garter snake (*Thamnophis sirtalis*) (Perry et al. 2018), corn snake (*Pantherophis guttatus*) (Ullate-Agote et al. 2014), mainland tiger snake, and king cobra (*Ophiophagus hannah*) (Vonk et al. 2013), and from genomic reads from pygmy rattlesnake and mountain garter snake (Vicoso et al. 2013a) (Supplemental Table S1 and Supplemental Data S1).

Phylogenetic analyses of ZW gene pairs reveal that mountain garter snake, five-pacer viper and pygmy rattlesnake share a common evolutionary stratum, containing 979 ancestral single-copy genes. This stratum formed after these three species diverged from the Arafura file snake, but before they diverged from each other, between 76 and 61.7 MYA (Fig. 1A, Supplemental Figs. S1 and S2, Supplemental Tables S3 and S6). We infer that one or more parallel strata including *WAC* and *CTNNB1* formed on the lineage leading to arafura file snake (Supplemental Figs. S1 and S2).

The most distal Z homologs of W-linked genes in this old stratum lie near an array of olfactory receptor genes (Supplemental Table S3). Similar arrays exist on the orthologous autosomes in chicken and human, indicating that this array is an ancestral feature of the amniote genome. This array is not fully resolved in the green anole lizard genome, and the lizard orthologs of more distal Z-linked genes are in unassigned scaffolds. Because W-linked genes were only predicted for orthologs of lizard Chromosome 6 (Yin et al 2016), *SNRNP70* from this stratum is the most distal Z–W pair predicted for five-pacer viper. However, the pseudoautosomal boundary of five-pacer viper maps to a much more distal location in prairie rattlesnake (Schield et al. 2019), so we infer that one or more additional strata must have formed in the lineage leading to five-pacer viper (Supplemental Fig. S1).

In mountain garter snake, 64 ancestral single-copy genes including *SRRM2* and *PTPRH* belong to a stratum that formed in the common ancestor of corn snake and mainland tiger snake (Supplemental Figs. S1 and S3, Supplemental Tables S3 and S6), around 51 MYA. Subsequently, around 48 MYA, a stratum containing 195 ancestral single-copy genes, including *PPP6R1* and *PRF1*, formed in the ancestor of mountain garter snake and corn snake (Supplemental Figs. S1 and S3, Supplemental Table S3). The remaining 62 single-copy genes map to the opposite side of an array of vomeronasal receptor genes and appear to be pseudoautosomal (Supplemental Fig, S3, Supplemental Tables S3 and S6). A parallel stratum, including *PPP6R1*, formed independently in the lineage leading to mainland tiger snake, but we could not resolve whether this predates the divergence with king cobra (Supplemental Figs. S1 and S3).

A stratum containing 214 genes, including *RASIP1* and *RPL18*, formed in the common ancestor of the pygmy rattlesnake and snakes from the *Crotalus* and *Protobothrops* genera (Supplemental Figs. S1 and S4, Supplemental Tables S3 and S6), around 29.5 MYA. This was followed by a stratum containing 45 genes, including *FLT3LG*, in the common ancestor of pygmy rattlesnake and timber rattlesnake (Supplemental Fig. S4, Supplemental Table S3), about 12.5 MYA. We infer that a parallel stratum containing *FLT3LG* formed in the common ancestor of Taiwan habu and Okinawa habu (Supplemental Figs. S1 and S4). Pygmy rattlesnake shares a common pseudoautosomal region boundary with the five-pacer viper and the prairie rattlesnake (Schield et al. 2019), near the same array of vomeronasal receptor genes as in garter snake. This suggests that this array of genes may participate in recurrent structural rearrangements that initiate stratum formation (Supplemental Fig. S4, Supplemental Tables S3 and S6).

Avian evolutionary strata

We reconciled published stratum assignments in birds (Handley et al. 2004; Vicoso et al. 2013b; Wright et al. 2014; Zhou et al. 2014; Xu et al. 2019a; Wang et al. 2019) with our new reconstruction of the ancestral gene order on the avian Z Chromosome (Supplemental Table S7 and S14).

We used ANGES (version 1.01) (Jones et al. 2012) to reconstruct the order of chicken orthologs on the ancestral autosome that evolved into the avian Z and W sex Chromosomes. We aligned the peptide sequences of chicken Z-linked genes from Ensembl (release 96)(Yates et al. 2019) to the reference genome assemblies of chicken (Hillier et al. 2004; Bellott et al. 2010), turkey (*Meleagris gallopavo*) (Dalloul et al. 2010), duck (*Anas platyrhynchos*) (Zhang et al. 2014), Anna's hummingbird (*Calypte anna*) (Zhang et al. 2014), great tit (*Parus major*) (Laine et al. 2016), common canary (*Serinus canaria*) (Frankl-Vilches et al. 2015), dark-eyed junco (*Junco hyemalis*) (Friis et al. 2018), ostrich (*Struthio camelus australis*) (Zhang et al. 2014), cassowary (*Casuarius casuarius*) (Sackton et al. 2019), emu (*Dromaius novaehollandiae*) (Sackton et al. 2019), white-throated tinamou (*Tinamus guttatus*) (Zhang et al. 2014), and Chilean tinamou (*Nothoprocta perdicaria*) (Sackton et al. 2019)], as well as the assemblies of American alligator (*Alligator mississippiensis*) (St

John et al. 2012), green anole lizard (Alföldi et al. 2011), and human (International Human Genome Sequencing Consortium 2004) genomes as outgroups (Supplemental Table S1). We recovered seven contiguous ancestral regions in the ancestor of birds.

The largest contiguous ancestral region contains 472 genes and stretches from the boundary between stratum 0 and stratum 1 to the pseudoautosomal region, and provides sufficient information to reconstruct all lineage-specific strata in birds (Supplemental Table S7 and S14). All other contiguous ancestral regions reside within stratum 0, which formed in the common ancestor of all birds and has been subject to extensive lineage-specific rearrangments on the Z Chromosome (Zhou et al. 2014). We made our best effort to reconstruct the ancestral gene order based on outgroup species within stratum 0, but our downstream analyses do not depend on the exact order of genes within this stratum.

Mammalian evolutionary strata

In mammals, we relied on published Y Chromosome sequence assemblies and reconstructions of evolutionary strata (Supplemental Table S15) (Lahn and Page 1999; Skaletsky et al. 2003; Ferrante et al. 2003; Murphy et al. 2007; Van Laere et al. 2008; Chang et al. 2011; Li et al. 2013; Bellott et al. 2014; Skinner et al. 2016; Janečka et al. 2018).

Distribution of survivors on ancestral autosomes

Out of 324 surviving ancestral genes on present-day W- and Y-Chromosomes, 118 survive alongside one or more neighbors from the ancestral autosome (Supplemental Table S7 & S16).

For each stratum in each species, we tallied the number of ancestral genes (g), and the number of survivor genes (s) that we observed adjacent to other survivors on the ancestral autosome (o_a), or isolated from other survivors (o_i). We calculated the expected number of isolated survivors (e_i) by:

$$e_i = round(s \times (1 - (s/g))^2)$$

and the expected number of adjacent survivors (e_a) by:

$$e_a = s - e_i$$

For all 107 species-stratum pairs with more than 2 survivors, we tested whether we observed significantly more adjacent survivors than expected by chance using a one-tailed Fisher's exact test on a 2x2 contingency table of the form:

	Observed	Expected
Adjacent	o_a	e_a
Isolated	o_i	e_i

Twelve species-stratum pairs were nominally significant at α = 0.05, but none were significant after applying Bonferroni correction for multiple testing (Supplemental Table S17).

Calculation of survival fraction

We calculated a gene-wise 'survival fraction' to fairly compare the longevity of surviving ancestral genes across X-Y and Z-W systems in different lineages with different numbers of sampled species and evolutionary strata of different ages.

We calculate the denominator by taking the total length, in millions of years, of all branches in the species tree (Supplemental Figure S1) where a gene could have been present on a sex-specific chromosome, taking into account the age of all evolutionary strata and X-to-Y transposition events (Supplemental Tables S18-23). For the numerator, we took the total length of the most parsimonious set of branches required to account for the survival of the gene in present-day species. The survival faction ranges from 0 (lost in all lineages) to 1 (survival in every possible lineage) (Supplemental Tables S7). In snakes, we chose to include prior information about the survival of RAB5A, WDR48, LSM12, COMMD3, MSL1, WAC, and CTNNB1 from species beyond five-pacer viper, pygmy rattlesnake, and mountain garter snake in our calculations (Supplemental Tables S2, S4 and S19-21). We illustrate the calculation of survival fraction with two selected examples from therian mammals.

Example 1: RBMX and RBMY

RBMX and RBMY began to diverge after the formation of therian stratum S1 about 159 million years ago (Supplemental Figure S1, Supplemental Tables S7, S15, and S23), and thus had the potential to survive in all therian mammals. Therefore the denominator is the sum of:

    6.7   (human to human-chimp ancestor)
    6.7   (chimp to human-chimp ancestor)
    1.9   (human-chimp ancestor to human-gorilla ancestor)
    8.6   (gorilla to human-gorilla ancestor)
    20.84 (human-gorilla ancestor to human-rhesus ancestor)
    29.44 (rhesus to human-rhesus ancestor)
    13.76 (human-rhesus ancestor to human-marmoset ancestor)

43.2   (marmoset to human-marmoset ancestor)
46.8   (human-marmoset ancestor to human-mouse ancestor)
20.9   (mouse to mouse-rat ancestor)
20.9   (rat to mouse-rat ancestor)
69.1   (mouse-rat ancestor to human-mouse ancestor)
6   (human-mouse ancestor to human-cattle ancestor)
55   (dog to dog-cat ancestor)
55   (cat to dog-cat ancestor)
22   (dog-cat ancestor to dog-horse ancestor)
77   (horse to dog-horse ancestor)
1   (dog-horse ancestor to dog-cattle ancestor)
62   (cattle to cattle-pig ancestor)
62   (pig to cattle-pig ancestor)
16   (cattle-pig ancestor to dog-cattle ancestor)
18   (dog-cattle ancestor to human-cattle ancestor)
63   (human-cattle ancestor to human-opossum ancestor)
82   (opossum to opossum-wallaby ancestor)
82   (wallaby to opossum-wallaby ancestor)
77   (opossum-wallaby ancestor to human-opossum ancestor)

Or a total of 966.84 MY.

RBMY survives in 13 of these 14 species, but was lost in cat. Therefore we calculate the numerator by taking the sum of:

6.7   (human to human-chimp ancestor)
6.7   (chimp to human-chimp ancestor)
1.9   (human-chimp ancestor to human-gorilla ancestor)
8.6   (gorilla to human-gorilla ancestor)
20.84   (human-gorilla ancestor to human-rhesus ancestor)
29.44   (rhesus to human-rhesus ancestor)
13.76   (human-rhesus ancestor to human-marmoset ancestor)
43.2   (marmoset to human-marmoset ancestor)
46.8   (human-marmoset ancestor to human-mouse ancestor)
20.9   (mouse to mouse-rat ancestor)
20.9   (rat to mouse-rat ancestor)
69.1   (mouse-rat ancestor to human-mouse ancestor)
6   (human-mouse ancestor to human-cattle ancestor)
55   (dog to dog-cat ancestor)
22   (dog-cat ancestor to dog-horse ancestor)
77   (horse to dog-horse ancestor)
1   (dog-horse ancestor to dog-cattle ancestor)
62   (cattle to cattle-pig ancestor)
62   (pig to cattle-pig ancestor)
16   (cattle-pig ancestor to dog-cattle ancestor)
18   (dog-cattle ancestor to human-cattle ancestor)

63	(human-cattle ancestor to human-opossum ancestor)
82	(opossum to opossum-wallaby ancestor)
82	(wallaby to opossum-wallaby ancestor)
77	(opossum-wallaby ancestor to human-opossum ancestor)

or a total of 911.84 MY, giving a survival fraction of 911.84/966.84 or 0.943113649.

Example 2: KDM5C and KDM5D

Many genes belong to multiple evolutionary strata that arose independently in different lineages. In this case, we sum the branch lengths from each independent stratum before taking the quotient. For example, KDM5D diverged from KDM5C independently in eutherian stratum 2/3 and metatherian stratum 2, about 96 and 82 million years ago, respectively (Supplemental Figure S1, Supplemental Tables S7, S15, and S23). In this case, we calculate the denominator by adding the lengths of the branches in the eutherian species tree, back to the human-cattle ancestor, to those in the metatherian species tree, back to the opossum-wallaby ancestor.

6.7	(human to human-chimp ancestor)
6.7	(chimp to human-chimp ancestor)
1.9	(human-chimp ancestor to human-gorilla ancestor)
8.6	(gorilla to human-gorilla ancestor)
20.84	(human-gorilla ancestor to human-rhesus ancestor)
29.44	(rhesus to human-rhesus ancestor)
13.76	(human-rhesus ancestor to human-marmoset ancestor)
43.2	(marmoset to human-marmoset ancestor)
46.8	(human-marmoset ancestor to human-mouse ancestor)
20.9	(mouse to mouse-rat ancestor)
20.9	(rat to mouse-rat ancestor)
69.1	(mouse-rat ancestor to human-mouse ancestor)
6	(human-mouse ancestor to human-cattle ancestor)
55	(dog to dog-cat ancestor)
22	(dog-cat ancestor to dog-horse ancestor)
1	(dog-horse ancestor to dog-cattle ancestor)
62	(cattle to cattle-pig ancestor)
62	(pig to cattle-pig ancestor)
16	(cattle-pig ancestor to dog-cattle ancestor)
18	(dog-cattle ancestor to human-cattle ancestor)

and

82	(opossum to opossum-wallaby ancestor)
82	(wallaby to opossum-wallaby ancestor)

for a total of 826.74 MY in the denominator.

KDM5D survived in 12 of these 14 species, but is absent from cattle and is a transcribed unprocessed pseudogene in pig. We infer that KDM5D was no longer functional after these two species diverged from dog, cat, and horse, but before they diverged from each other. Therefore, we calculate the numerator by taking the sum of:

6.7   (human to human-chimp ancestor)
6.7   (chimp to human-chimp ancestor)
1.9   (human-chimp ancestor to human-gorilla ancestor)
8.6   (gorilla to human-gorilla ancestor)
20.84 (human-gorilla ancestor to human-rhesus ancestor)
29.44 (rhesus to human-rhesus ancestor)
13.76 (human-rhesus ancestor to human-marmoset ancestor)
43.2   (marmoset to human-marmoset ancestor)
46.8   (human-marmoset ancestor to human-mouse ancestor)
20.9   (mouse to mouse-rat ancestor)
20.9   (rat to mouse-rat ancestor)
69.1   (mouse-rat ancestor to human-mouse ancestor)
6   (human-mouse ancestor to human-cattle ancestor)
55   (dog to dog-cat ancestor)
22   (dog-cat ancestor to dog-horse ancestor)
1   (dog-horse ancestor to dog-cattle ancestor)
18   (dog-cattle ancestor to human-cattle ancestor)

and

82   (opossum to opossum-wallaby ancestor)
82   (wallaby to opossum-wallaby ancestor)

for a total of 686.74 MY, giving a survival fraction of 686.74/826.74 or 0.830660183.

SUPPLEMENTAL REFERENCES

Aird SD, Arora J, Barua A, Qiu L, Terada K, Mikheyev AS. 2017. Population Genomic Analysis of a Pitviper Reveals Microevolutionary Forces Underlying Venom Chemistry. *Genome Biology and Evolution* **9**: 2640–2649.

Alföldi J, Di Palma F, Grabherr M, Williams C, Kong L, Mauceli E, Russell P, Lowe CB, Glor RE, Jaffe JD, et al. 2011. The genome of the green anole lizard and a comparative analysis with birds and mammals. *Nature* **477**: 587–591.

Cai Q, Qian X, Lang Y, Luo Y, Xu J, Pan S, Hui Y, Gou C, Cai Y, Hao M, et al. 2013. Genome sequence of ground tit Pseudopodoces humilis and its adaptation to high altitude. *Genome Biol* **14**: R29.

Castoe TA, de Koning APJ, Hall KT, Card DC, Schield DR, Fujita MK, Ruggiero RP, Degner JF, Daza JM, Gu W, et al. 2013. The Burmese python genome reveals the molecular basis for extreme adaptation in snakes. *Proceedings of the National Academy of Sciences* **110**: 20645–20650.

Chakraborty S, Rafi MA, Wenger DA. 1994. Mutations in the lysosomal beta-galactosidase gene that cause the adult form of GM1 gangliosidosis. *Am J Hum Genet* **54**: 1004–1013.

Chang T-C, Klabnik JL, Liu W-S. 2011. Regional Selection Acting on the OFD1 Gene Family. *PLoS ONE* **6**: e26195.

Dalloul RA, Long JA, Zimin AV, Aslam L, Beal K, Blomberg LA, Bouffard P, Burt DW, Crasta O, Crooijmans RPMA, et al. 2010. Multi-platform next-generation sequencing of the domestic turkey (Meleagris gallopavo): Genome assembly and analysis. *PLoS biology* **8**.

Elgvin TO, Trier CN, Tørresen OK, Hagen IJ, Lien S, Nederbragt AJ, Ravinet M, Jensen H, Sætre G-P. 2017. The genomic mosaicism of hybrid speciation. *Sci Adv* **3**: e1602996.

Ellegren H, Smeds L, Burri R, Olason PI, Backström N, Kawakami T, Künstner A, Mäkinen H, Nadachowska-Brzyska K, Qvarnström A, et al. 2012. The genomic landscape of species divergence in Ficedula flycatchers. *Nature* **491**: 756–760.

Felsenstein J. 1989. PHYLIP- phylogeny inference package, version. 3. 2. *Cladistics* **5**: 163–166.

Ferrante MI, Barra A, Truong J-P, Banfi S, Disteche CM, Franco B. 2003. Characterization of the OFD1/Ofd1 genes on the human and mouse sex chromosomes and exclusion of Ofd1 for the Xpl mouse mutant73. *Genomics* **81**: 560–569.

Frankl-Vilches C, Kuhl H, Werber M, Klages S, Kerick M, Bakker A, de Oliveira EH, Reusch C, Capuano F, Vowinckel J, et al. 2015. Using the canary genome to decipher the evolution of hormone-sensitive gene regulation in seasonal singing birds. *Genome Biology* **16**: 19.

Friis G, Fandos G, Zellmer AJ, McCormack JE, Faircloth BC, Milá B. 2018. Genome-wide signals of drift and local adaptation during rapid lineage divergence in a songbird. *Molecular Ecology* **27**: 5137–5153.

Gilbert C, Meik JM, Dashevsky D, Card DC, Castoe TA, Schaack S. 2014. Endogenous hepadnaviruses, bornaviruses and circoviruses in snakes. *Proceedings of the Royal Society B: Biological Sciences* **281**: 20141122.

Gonzalez MA, Feely SM, Speziani F, Strickland AV, Danzi M, Bacon C, Lee Y, Chou T-F, Blanton SH, Weihl CC, et al. 2014. A novel mutation in VCP causes Charcot-Marie-Tooth Type 2 disease. *Brain* **137**: 2897–2902.

Gordon D, Huddleston J, Chaisson MJP, Hill CM, Kronenberg ZN, Munson KM, Malig M, Raja A, Fiddes I, Hillier LW, et al. 2016. Long-read sequence assembly of the gorilla genome. *Science* **352**: aae0344–aae0344.

Groenen MAM, Archibald AL, Uenishi H, Tuggle CK, Takeuchi Y, Rothschild MF, Rogel-Gaillard C, Park C, Milan D, Megens H-J, et al. 2012. Analyses of pig genomes provide insight into porcine demography and evolution. *Nature* **491**: 393–398.

Haeussler M, Zweig AS, Tyner C, Speir ML, Rosenbloom KR, Raney BJ, Lee CM, Lee BT, Hinrichs AS, Gonzalez JN, et al. 2019. The UCSC Genome Browser database: 2019 update. *Nucleic Acids Research* **47**: D853–D858.

Hillier LW, Miller W, International Chicken Genome Sequencing Consortium. 2004. Sequence and comparative analysis of the chicken genome provide unique perspectives on vertebrate evolution. *Nature* **432**: 695–716.

International Human Genome Sequencing Consortium. 2004. Finishing the euchromatic sequence of the human genome. *Nature* **431**: 931–945.

Johnson JO, Mandrioli J, Benatar M, Abramzon Y, Van Deerlin VM, Trojanowski JQ, Gibbs JR, Brunetti M, Gronka S, Wuu J, et al. 2010. Exome sequencing reveals VCP mutations as a cause of familial ALS. *Neuron* **68**: 857–864.

Jones BR, Rajaraman A, Tannier E, Chauve C. 2012. ANGES: Reconstructing ANcestral GEnomeS maps. *Bioinformatics* **28**: 2388–2390.

Kato J, Fujikawa K, Kanda M, Fukuda N, Sasaki K, Takayama T, Kobune M, Takada K, Takimoto R, Hamada H, et al. 2001. A mutation, in the iron-responsive element of H ferritin mRNA, causing autosomal dominant iron overload. *Am J Hum Genet* **69**: 191–197.

Kent WJ. 2002. BLAT–the BLAST-like alignment tool. *Genome Research* **12**: 656–664.

Kielbasa SM, Wan R, Sato K, Horton P, Frith MC. 2011. Adaptive seeds tame genomic sequence comparison. *Genome Research* **21**: 487–493.

Kishi H, Mukai T, Hirono A, Fujii H, Miwa S, Hori K. 1987. Human aldolase A deficiency associated with a hemolytic anemia: thermolabile aldolase due to a single base mutation. *Proc Natl Acad Sci USA* **84**: 8623–8627.

Laine VN, Gossmann TI, Schachtschneider KM, Garroway CJ, Madsen O, Verhoeven KJF, de Jager V, Megens H-J, Warren WC, Minx P, et al. 2016. Evolutionary signals of selection on cognition from the great tit genome and methylome. *Nature Communications* **7**: 10474.

Langmead B, Trapnell C, Pop M, Salzberg SL. 2009. Ultrafast and memory-efficient alignment of short DNA sequences to the human genome. *Genome Biology* **10**: R25.

Lindblad-Toh K, Wade CM, Mikkelsen TS, Karlsson EK, Jaffe DB, Kamal M, Clamp M, Chang JL, Kulbokas EJ, Zody MC, et al. 2005. Genome sequence, comparative analysis and haplotype structure of the domestic dog. *Nature* **438**: 803–819.

Matsubara K, Kuraku S, Tarui H, Nishimura O, Nishida C, Agata K, Kumazawa Y, Matsuda Y. 2012. Intra-genomic GC heterogeneity in sauropsids: Evolutionary insights from cDNA mapping and GC3 profiling in snake. *BMC Genomics* **13**: 604.

McKoy G, Protonotarios N, Crosby A, Tsatsopoulou A, Anastasakis A, Coonar A, Norman M, Baboonian C, Jeffery S, McKenna WJ. 2000. Identification of a deletion in plakoglobin in arrhythmogenic right ventricular cardiomyopathy with palmoplantar keratoderma and woolly hair (Naxos disease). *The Lancet* **355**: 2119–2124.

Mikkelsen TS, Broad Institute Genome Sequencing Platform, Broad Institute Whole Genome Assembly Team, Wakefield MJ, Aken B, Amemiya CT, Chang JL, Duke S, Garber M, Gentles AJ, et al. 2007. Genome of the marsupial Monodelphis domestica reveals innovation in non-coding sequences. *Nature* **447**: 167–177.

Moortgat S, Berland S, Aukrust I, Maystadt I, Baker L, Benoit V, Caro-Llopis A, Cooper NS, Debray F-G, Faivre L, et al. 2018. HUWE1 variants cause dominant X-linked intellectual disability: A clinical study of 21 patients. *European journal of human genetics: EJHG* **26**: 64–74.

Mouse Genome Sequencing Consortium. 2002. Initial sequencing and comparative analysis of the mouse genome. *Nature* **420**: 520–562.

Murphy WJ, Davis B, David VA, Agarwala R, Schäffer AA, Pearks Wilkerson AJ, Neelam B, O'Brien SJ, Menotti-Raymond M. 2007. A 1.5-Mb-resolution radiation hybrid map of the cat genome and comparative analysis with the canine and human genomes. *Genomics* **89**: 189–196.

Murtagh VJ, O'Meally D, Sankovic N, Delbridge ML, Kuroki Y, Boore JL, Toyoda A, Jordan KS, Pask AJ, Renfree MB, et al. 2012. Evolutionary history of novel genes on

the tammar wallaby Y chromosome: Implications for sex chromosome evolution. *Genome Research* **22**: 498–507.

Nishimoto J, Nanba E, Inui K, Okada S, Suzuki K. 1991. GM1-gangliosidosis (genetic beta-galactosidase deficiency): identification of four mutations in different clinical phenotypes among Japanese patients. *Am J Hum Genet* **49**: 566–574.

Oshima A, Yoshida K, Shimmoto M, Fukuhara Y, Sakuraba H, Suzuki Y. 1991. Human beta-galactosidase gene mutations in morquio B disease. *Am J Hum Genet* **49**: 1091–1093.

Pontius JU, Mullikin JC, Smith DR, Agencourt Sequencing Team, Lindblad-Toh K, Gnerre S, Clamp M, Chang J, Stephens R, Neelam B, et al. 2007. Initial sequence and comparative analysis of the cat genome. *Genome Research* **17**: 1675–1689.

Quinlan AR, Hall IM. 2010. BEDTools: A flexible suite of utilities for comparing genomic features. *Bioinformatics* **26**: 841–842.

Rat Genome Sequencing Project Consortium. 2004. Genome sequence of the Brown Norway rat yields insights into mammalian evolution. *Nature* **428**: 493–521.

Renfree MB, Papenfuss AT, Deakin JE, Lindsay J, Heider T, Belov K, Rens W, Waters PD, Pharo EA, Shaw G, et al. 2011. Genome sequence of an Australian kangaroo, Macropus eugenii, provides insight into the evolution of mammalian reproduction and development. *Genome Biol* **12**: R81.

Rhesus Macaque Genome Sequencing and Analysis Consortium, Gibbs RA, Rogers J, Katze MG, Bumgarner R, Weinstock GM, Mardis ER, Remington KA, Strausberg RL, Venter JC, et al. 2007. Evolutionary and Biomedical Insights from the Rhesus Macaque Genome. *Science* **316**: 222–234.

Sackton TB, Grayson P, Cloutier A, Hu Z, Liu JS, Wheeler NE, Gardner PP, Clarke JA, Baker AJ, Clamp M, et al. 2019. Convergent regulatory evolution and loss of flight in paleognathous birds. *Science* **364**: 74–78.

Schmidt HA, Strimmer K, Vingron M, von Haeseler A. 2002. TREE-PUZZLE: Maximum likelihood phylogenetic analysis using quartets and parallel computing. *Bioinformatics* **18**: 502–504.

Shibata H, Chijiwa T, Oda-Ueda N, Nakamura H, Yamaguchi K, Hattori S, Matsubara K, Matsuda Y, Yamashita A, Isomoto A, et al. 2018. The habu genome reveals accelerated evolution of venom protein genes. *Scientific Reports* **8**: 11300.

Shimodaira H, Hasegawa M. 1999. Multiple Comparisons of Log-Likelihoods with Applications to Phylogenetic Inference. *Molecular Biology and Evolution* **16**: 1114–1116.

Sievers F, Wilm A, Dineen D, Gibson TJ, Karplus K, Li W, Lopez R, McWilliam H, Remmert M, Söding J, et al. 2011. Fast, scalable generation of high-quality protein

multiple sequence alignments using Clustal Omega. *Molecular Systems Biology* **7**: 539.

Sifrim A, the INTERVAL Study, the UK10K Consortium, the Deciphering Developmental Disorders Study, Hitz M-P, Wilsdon A, Breckpot J, Turki SHA, Thienpont B, McRae J, et al. 2016. Distinct genetic architectures for syndromic and nonsyndromic congenital heart defects identified by exome sequencing. *Nature Genetics* **48**: 1060–1065.

Slater G, Birney E. 2005. Automated generation of heuristics for biological sequence comparison. *BMC Bioinformatics* **6**: 31.

Smeds L, Warmuth V, Bolivar P, Uebbing S, Burri R, Suh A, Nater A, Bureš S, Garamszegi LZ, Hogner S, et al. 2015. Evolutionary analysis of the female-specific avian W chromosome. *Nat Commun* **6**: 7330.

Snijders Blok L, Madsen E, Juusola J, Gilissen C, Baralle D, Reijnders MRF, Venselaar H, Helsmoortel C, Cho MT, Hoischen A, et al. 2015. Mutations in DDX3X Are a Common Cause of Unexplained Intellectual Disability with Gender-Specific Effects on Wnt Signaling. *American Journal of Human Genetics* **97**: 343–352.

Soh YQS, Alföldi J, Pyntikova T, Brown LG, Graves T, Minx PJ, Fulton RS, Kremitzki C, Koutseva N, Mueller JL, et al. 2014. Sequencing the mouse Y chromosome reveals convergent gene acquisition and amplification on both sex chromosomes. *Cell* **159**: 800–813.

St John JA, Braun EL, Isberg SR, Miles LG, Chong AY, Gongora J, Dalzell P, Moran C, Bed'hom B, Abzhanov A, et al. 2012. Sequencing three crocodilian genomes to illuminate the evolution of archosaurs and amniotes. *Genome Biology* **13**: 415.

Suyama M, Torrents D, Bork P. 2006. PAL2NAL: Robust conversion of protein sequence alignments into the corresponding codon alignments. *Nucleic Acids Research* **34**: W609–W612.

The Bovine Genome Sequencing and Analysis Consortium, Elsik CG, Tellam RL, Worley KC, Gibbs RA, Muzny DM, Weinstock GM, Adelson DL, Eichler EE, Elnitski L, et al. 2009. The Genome Sequence of Taurine Cattle: A Window to Ruminant Biology and Evolution. *Science* **324**: 522–528.

The Chimpanzee Sequencing and Analysis Consortium. 2005. Initial sequence of the chimpanzee genome and comparison with the human genome. *Nature* **437**: 69–87.

The Marmoset Genome Sequencing and Analysis Consortium. 2014. The common marmoset genome provides insight into primate biology and evolution. *Nat Genet* **46**: 850–857.

Tomaszkiewicz M, Rangavittal S, Cechova M, Sanchez RC, Fescemyer HW, Harris R, Ye D, O'Brien PCM, Chikhi R, Ryder OA, et al. 2016. A time- and cost-effective

strategy to sequence mammalian Y Chromosomes: an application to the de novo assembly of gorilla Y. *Genome Res* **26**: 530–540.

Ullate-Agote A, Milinkovitch MC, Tzika AC. 2014. The genome sequence of the corn snake (Pantherophis guttatus), a valuable resource for EvoDevo studies in squamates. *The International Journal of Developmental Biology* **58**: 881–888.

Van Laere A-S, Coppieters W, Georges M. 2008. Characterization of the bovine pseudoautosomal boundary: Documenting the evolutionary history of mammalian sex chromosomes. *Genome Research* **18**: 1884–1895.

Vicoso B, Kaiser VB, Bachtrog D. 2013b. Sex-biased gene expression at homomorphic sex chromosomes in emus and its implication for sex chromosome evolution. *Proceedings of the National Academy of Sciences* **110**: 6453–6458.

Vonk FJ, Casewell NR, Henkel CV, Heimberg AM, Jansen HJ, McCleary RJR, Kerkkamp HME, Vos RA, Guerreiro I, Calvete JJ, et al. 2013. The king cobra genome reveals dynamic gene evolution and adaptation in the snake venom system. *Proceedings of the National Academy of Sciences* **110**: 20651–20656.

Wade CM, Giulotto E, Sigurdsson S, Zoli M, Gnerre S, Imsland F, Lear TL, Adelson DL, Bailey E, Bellone RR, et al. 2009. Genome Sequence, Comparative Analysis, and Population Genetics of the Domestic Horse. *Science* **326**: 865–867.

Wang Z, Zhang J, Xu X, Witt C, Deng Y, Chen G, Meng G, Feng S, Szekely T, Zhang G, et al. 2019. *Phylogeny, transposable element and sex chromosome evolution of the basal lineage of birds*. Evolutionary Biology.

Warren WC, Clayton DF, Ellegren H, Arnold AP, Hillier LW, Künstner A, Searle S, White S, Vilella AJ, Fairley S, et al. 2010. The genome of a songbird. *Nature* **464**: 757–762.

Watts GDJ, Wymer J, Kovach MJ, Mehta SG, Mumm S, Darvish D, Pestronk A, Whyte MP, Kimonis VE. 2004. Inclusion body myopathy associated with Paget disease of bone and frontotemporal dementia is caused by mutant valosin-containing protein. *Nat Genet* **36**: 377–381.

Wicker G, Prill V, Brooks D, Gibson G, Hopwood J, von Figura K, Peters C. 1991. Mucopolysaccharidosis VI (Maroteaux-Lamy syndrome). An intermediate clinical phenotype caused by substitution of valine for glycine at position 137 of arylsulfatase B. *J Biol Chem* **266**: 21386–21391.

Williams SR, Gekeler V, McIvor RS, Martin DW. 1987. A human purine nucleoside phosphorylase deficiency caused by a single base change. *J Biol Chem* **262**: 2332–2338.

Wright AE, Harrison PW, Montgomery SH, Pointer MA, Mank JE. 2014. Independent stratum formation on the avian sex chromosomes reveals inter-chromosomal gene

conversion and predominance of purifying selection on the W chromosome: Sex chromosome evolution. *Evolution* **68**: 3281–3295.

Xu L, Wa Sin SY, Grayson P, Edwards SV, Sackton TB. 2019b. Evolutionary Dynamics of Sex Chromosomes of Paleognathous Birds. *Genome Biology and Evolution* **11**: 2376–2390.

Zhou Q, Zhang J, Bachtrog D, An N, Huang Q, Jarvis ED, Gilbert MTP, Zhang G. 2014. Complex evolutionary trajectories of sex chromosomes across bird taxa. *Science* **346**: 1246338–1246338.
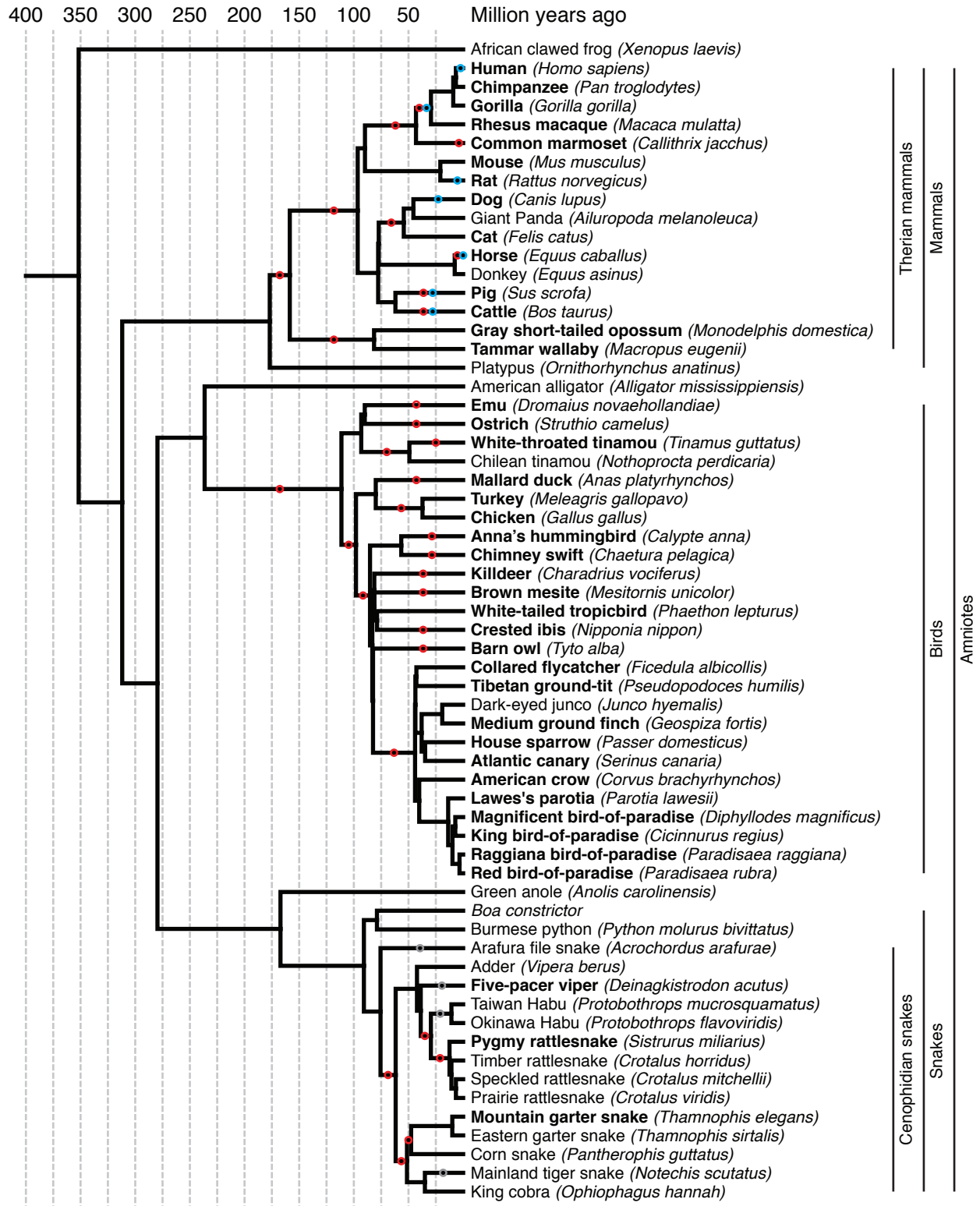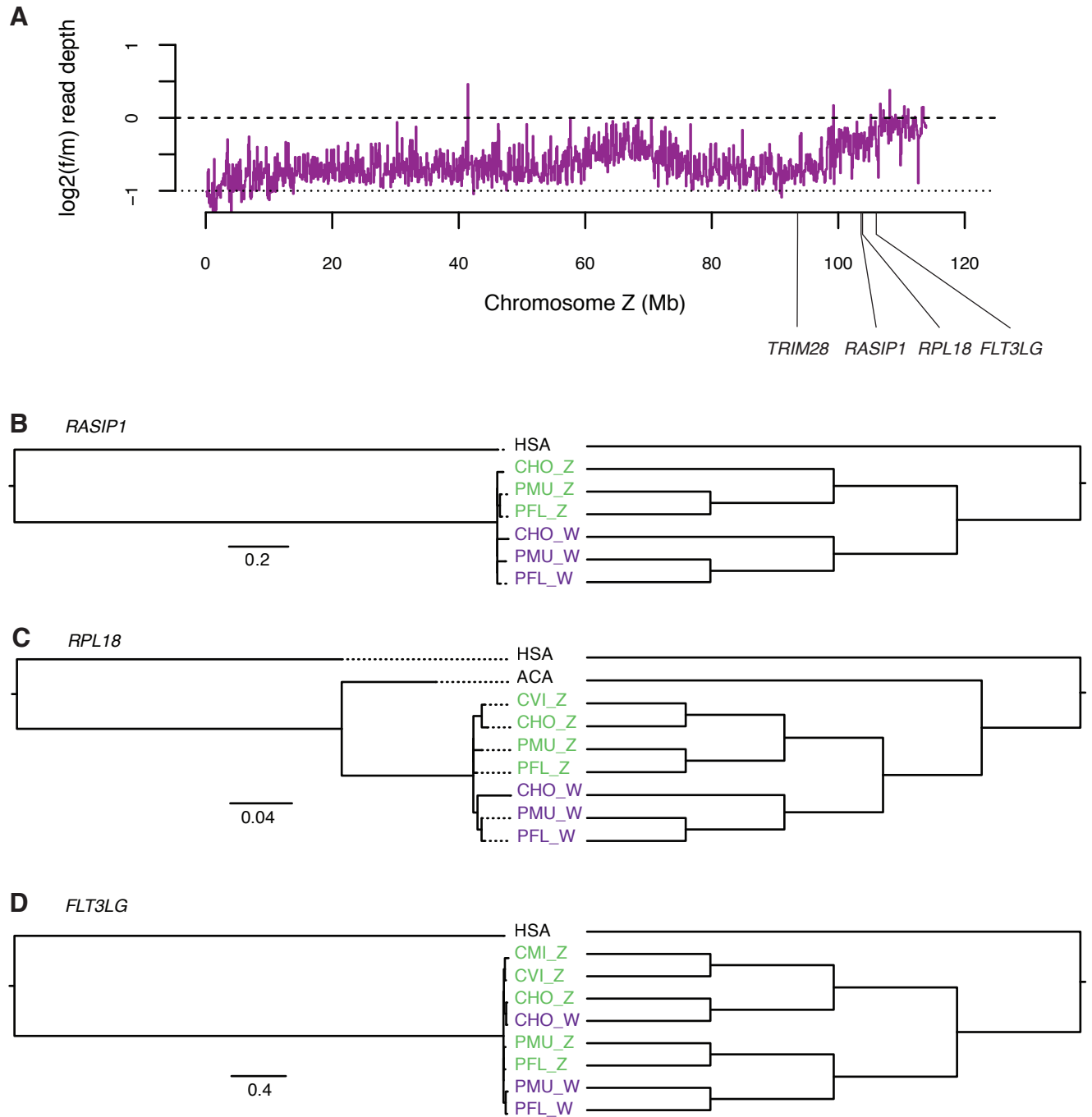
Supplemental Figure S1. Phylogenetic tree of selected amniote species. Phylogenetic tree of amniote species used in this study from TimeTree (Kumar et al. 2017). Species with systematic gene predictions from sex-specific W or Y chromosomes in bold. Red circles mark branches with evolutionary strata with defined boundaries. Blue circles mark branches with X-to-Y transposition events that restored lost ancestral genes to the Y chromosome. Grey circles mark branches with evolutionary strata inferred from phylogenetic analyses of Z–W pairs in snakes, with unknown boundaries. See also Supplemental Tables S6, S14, & S15.
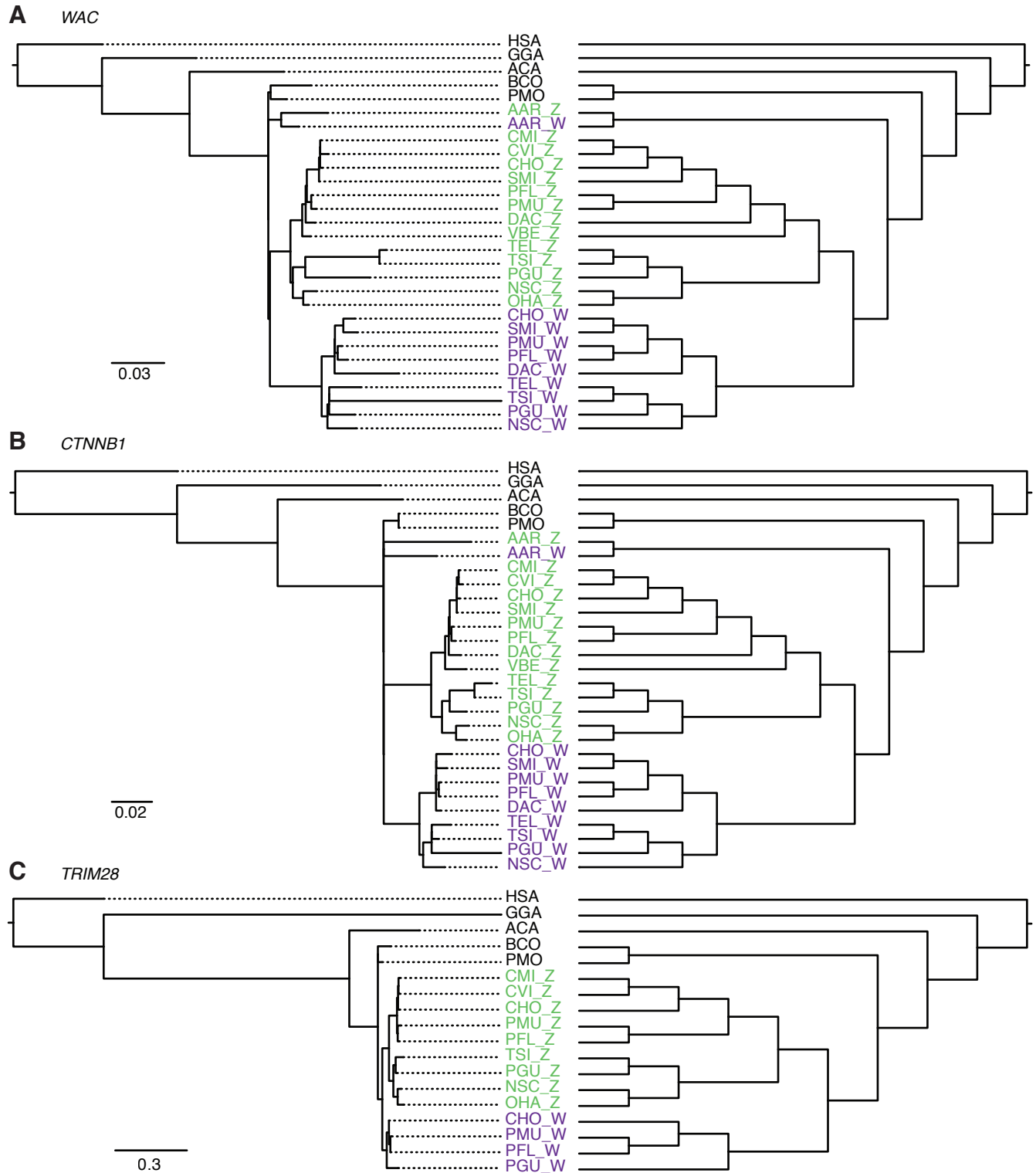
Supplemental Figure S2. A large evolutionary stratum formed after vipers and colubroid snakes diverged from Arafura file snake. Best supported gene trees from maximum likelihood and parsimony analysis of representative genes (A) *WAC*, (B) *CTNNB1*, and (C) *TRIM28*. Purple, W-linked homologs; green Z-linked homologs; black, autosomal homologs. Left, maximum likelihood tree; scale bars represent expected number of nucleotide substitutions per site along each branch. Right, cladograms to show topology of short branches. Species abbreviations: HSA, human; GGA, chicken; ACA, lizard; BCO, Boa constrictor; PMO, python; AAR, Arafura file snake; CMI, speckled rattlesnake; CVI, prairie rattlesnake; CHO, timber rattlesnake; SMI, pygmy rattlesnake; PFL, Okinawa habu; PMU, Taiwan habu; DAC, five-pacer viper; VBE, adder; TEL, mountain garter snake; TSI, eastern garter snake; PGU, corn snake; NSC, mainland tiger snake; OHA, king cobra.
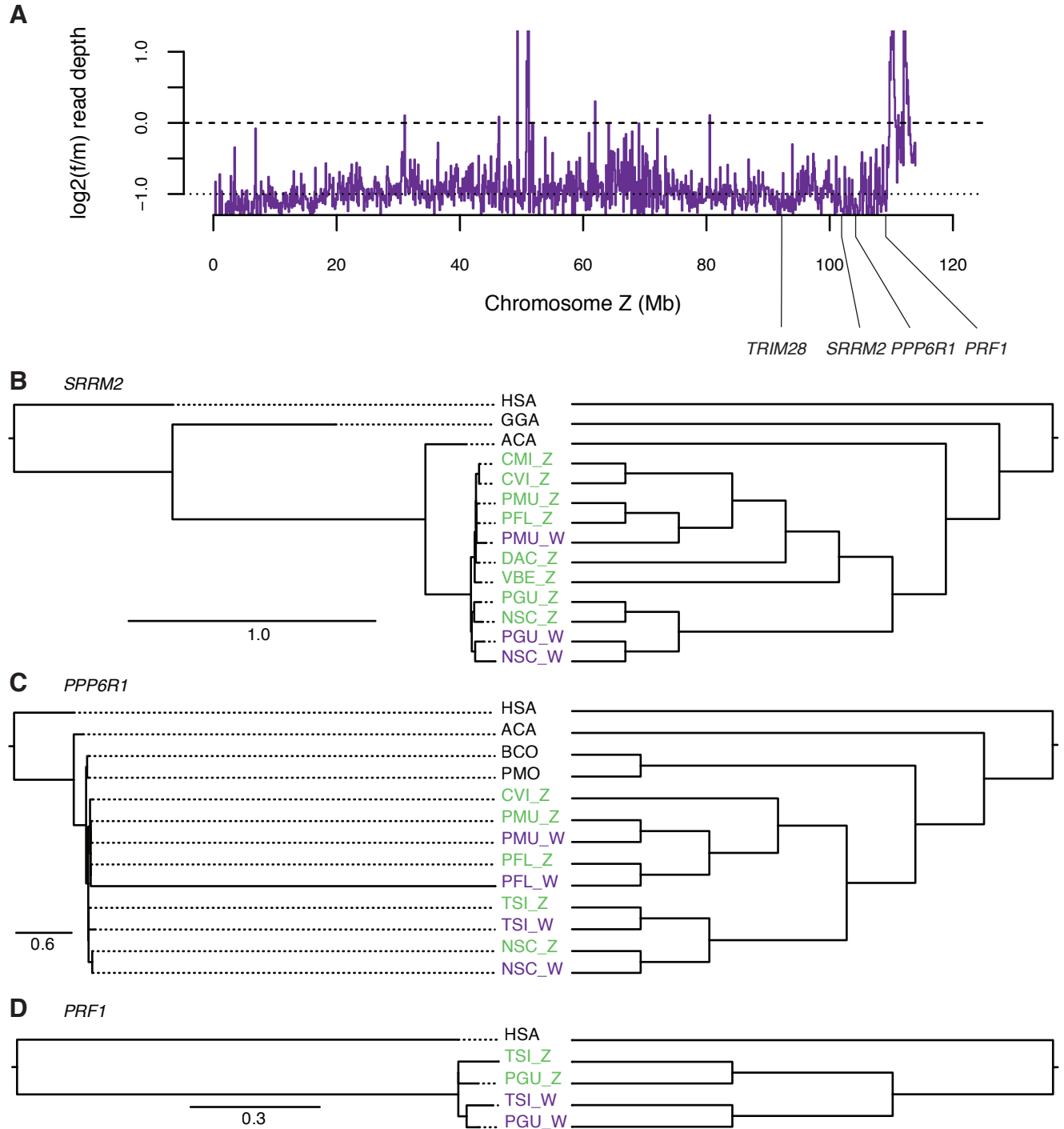
Supplemental Figure S3. Lineage specific strata in mountain garter snake. (A) Log2 normalized female/male coverage ratio of mountain garter snake mapped to the prairie rattlesnake reference genome in 100kb windows. The dashed line at zero represents expectation for diploid sequence; the dotted line at -1 represents the expectation of hemizygous sequence. Best supported gene trees from maximum likelihood and parsimony analysis of (B) *SRRM2*, (C) *PPP6R1*, and (D) *PRF1*. Purple, W-linked homologs; green Z-linked homologs; black, autosomal homologs. Left, maximum likelihood tree; scale bars represent expected number of nucleotide substitutions per site along each branch. Right, cladograms to show topology of short branches. Species abreviations: HSA, human; GGA, chicken; ACA, lizard; BCO, Boa constrictor; PMO, python; AAR, Arafura file snake; CMI, speckled rattlesnake; CVI, prairie rattlesnake; CHO, timber rattlesnake; SMI, pygmy rattlesnake; PFL, Okinawa habu; PMU, Taiwan habu; DAC, five-pacer viper; VBE, adder; TEL, mountain garter snake; TSI, eastern garter snake; PGU, corn snake; NSC, mainland tiger snake; OHA, king cobra.

Supplemental Figure S4. Lineage specific strata in pygmy rattlesnake. (A) Log2 normalized female/male coverage ratio of pygmy rattlesnake mapped to the prairie rattlesnake reference genome in 100kb windows. The dashed line at zero represents expectation for diploid sequence; the dotted line at -1 represents the expectation of hemizygous sequence. Best supported gene trees from maximum likelihood and parsimony analysis of (B) *RASIP1*, (C) *RPL18*, and (D) *FLT3LG*. Purple, W-linked homologs; green Z-linked homologs; black, autosomal homologs. Left, maximum likelihood tree; scale bars represent expected number of nucleotide substitutions per site along each branch. Right, cladograms to show topology of short branches. Species abreviations: HSA, human; GGA, chicken; ACA, lizard; BCO, Boa constrictor; PMO, python; AAR, Arafura file snake; CMI, speckled rattlesnake; CVI, prairie rattlesnake; CHO, timber rattlesnake; SMI, pygmy rattlesnake; PFL, Okinawa habu; PMU, Taiwan habu; DAC, five-pacer viper; VBE, adder; TEL, mountain garter snake; TSI, eastern garter snake; PGU, corn snake; NSC, mainland tiger snake; OHA, king cobra.
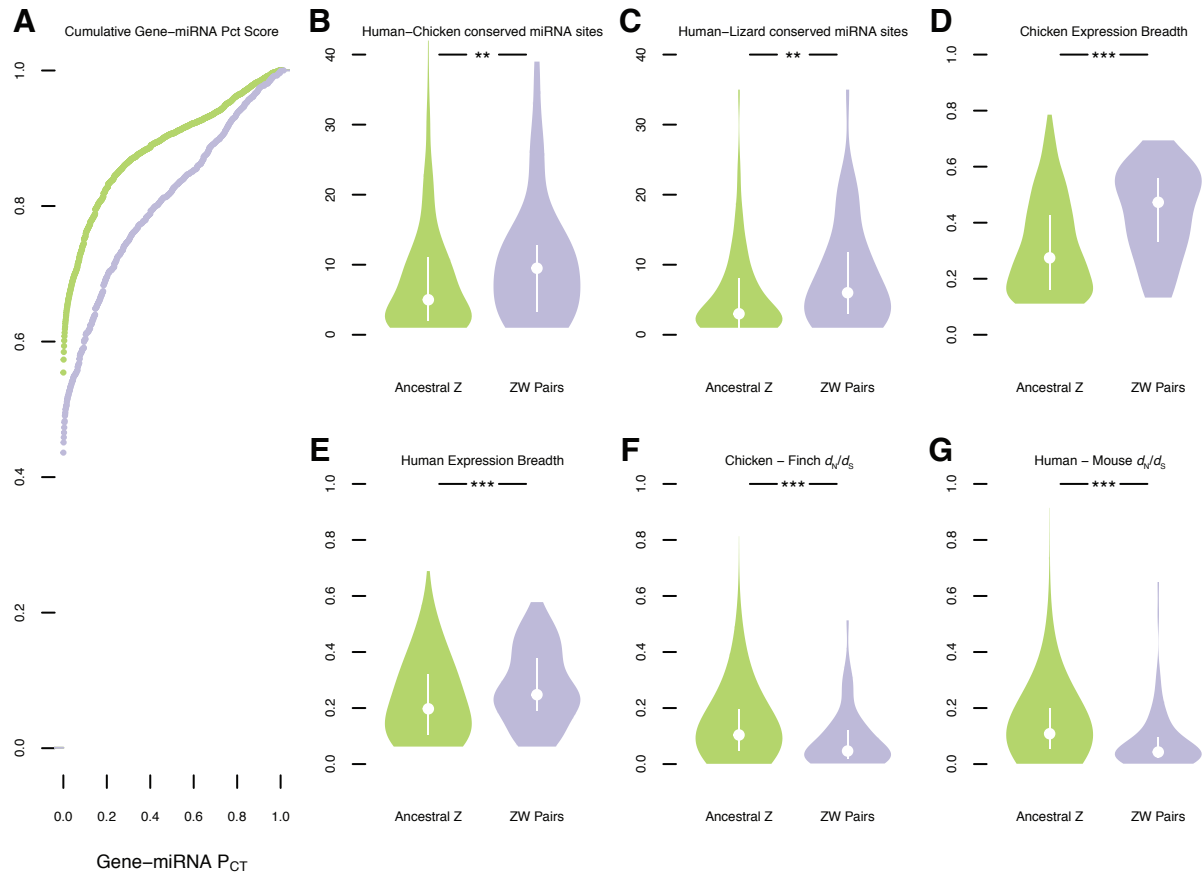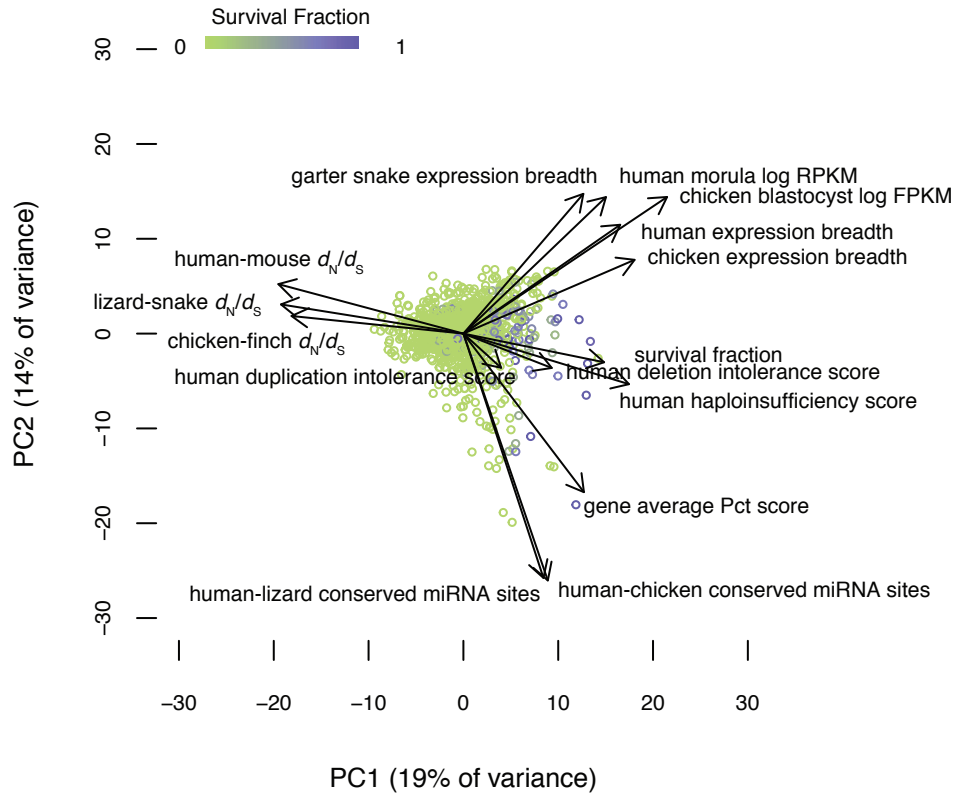
Supplemental Figure S5. Additional factors in the survival of caenophidian Z–W gene pairs. (**) P < 0.01, (***) P < 0.001. Cumulative distribution plot, showing human orthologs of ancestral caenophidian Z–W gene pairs have greater (A) PCT scores across all gene–miRNA interactions involving human orthologs of ancestral Z–W gene pairs (purple) than the remainder of ancestral Z genes (green) (two-sided Kolmogorov–Smirnov test). Violin plots, with the median (white circle) and interquartile range (white bar) indicated, compare annotations of ancestral Z–W gene pairs identified in 3 species (purple) to annotations for the remainder of ancestral Z genes (green). P values obtained using one-tailed Mann–Whitney U tests. See Methods and Supplemental Table 5. Human orthologs of ancestral Z–W gene pairs have more miRNA sites conserved between 3′ UTRs of (B) human and chicken orthologs and (C) human and lizard orthologs than do other ancestral Z genes. Orthologs of ancestral Z–W gene pairs are more broadly expressed than orthologs of other ancestral Z genes (D) in a panel of eight adult chicken tissues, and (E) in a panel of eight adult human tissues. Orthologs of ancestral Z–W gene pairs have reduced d_N/d_S ratios compared to orthologs of other ancestral Z genes in alignments between (F) chicken and zebra finch orthologs, and (G) human and mouse orthologs.
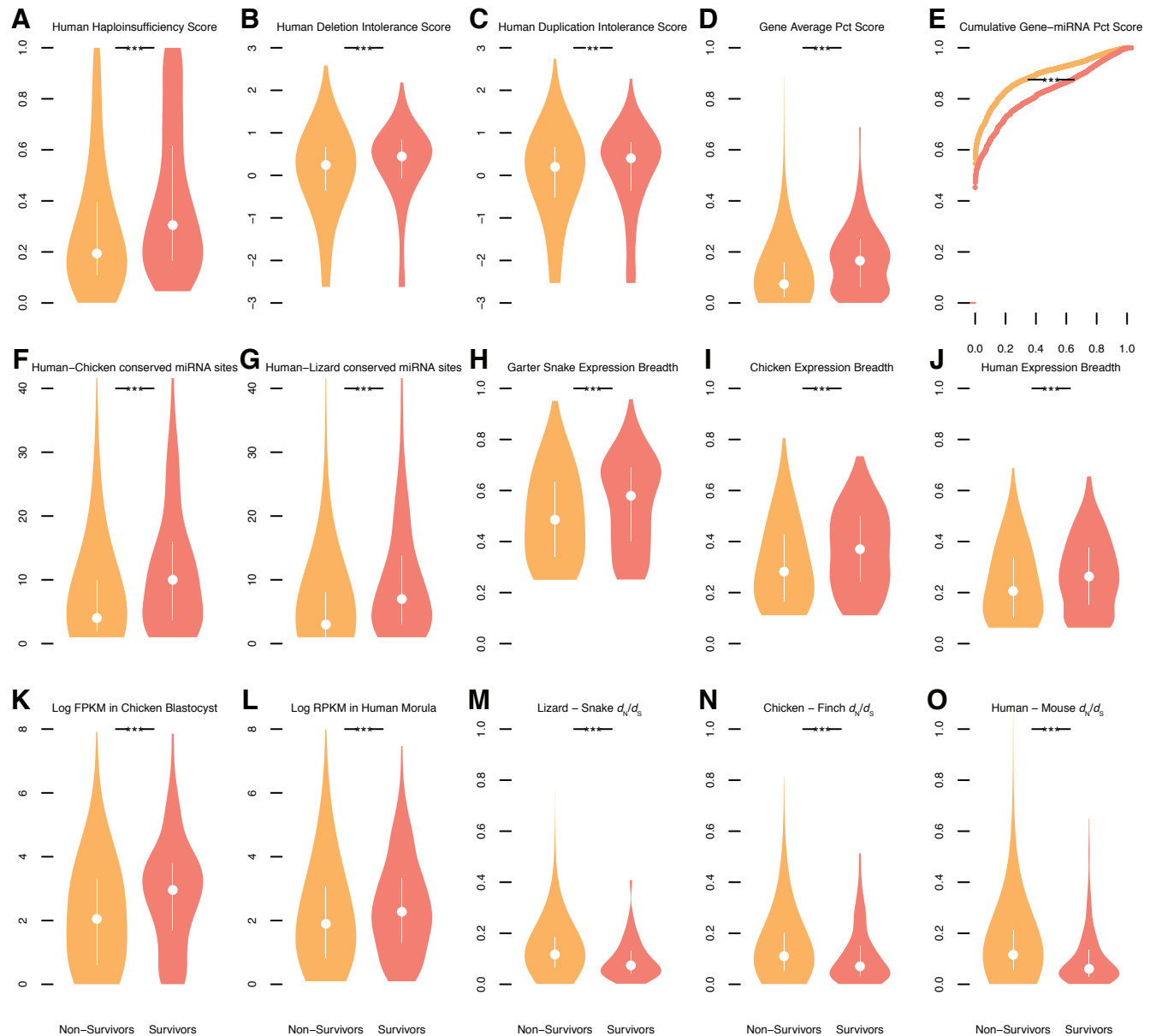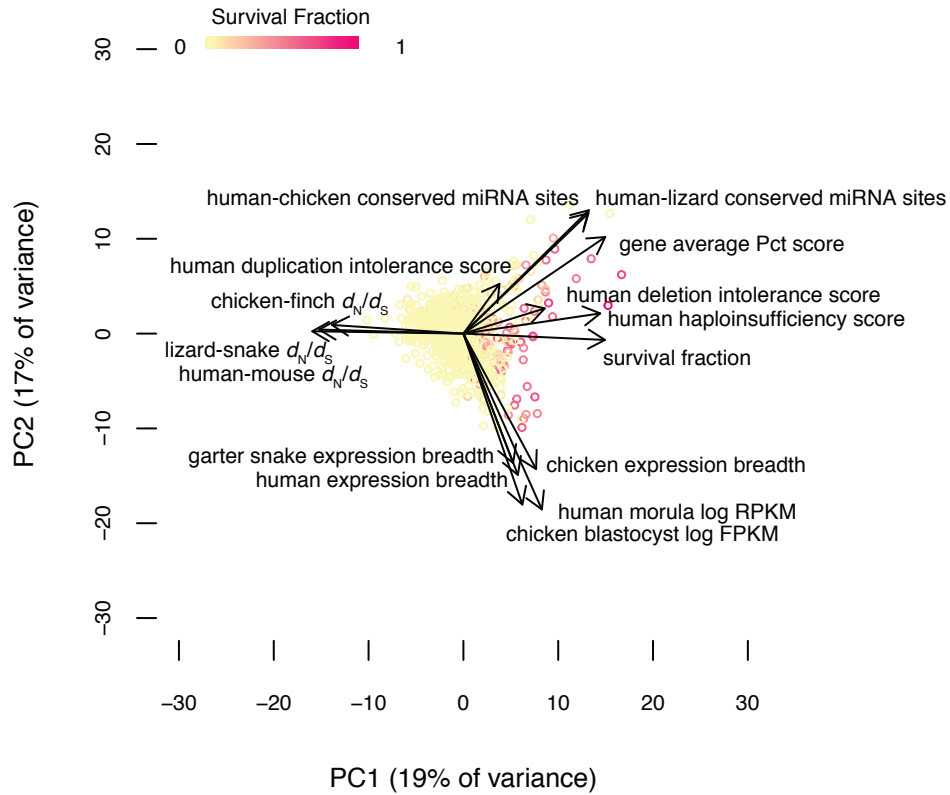
Supplemental Figure S6. Factors in the survival of amniote X–Y and Z–W gene pairs. Violin plots, with the median (white circle) and interquartile range (white bar) indicated, compare annotations of surviving ancestral X–Y and Z–W gene pairs identified in 41 amniote species (red) to annotations for the remainder of ancestral X or Z genes (orange). (**) P < 0.01, (***) P < 0.001. Unless otherwise noted, P values were obtained using one-tailed Mann–Whitney U tests. See Methods and Supplemental Table 5. Human orthologs of survivors have greater (A) probability of haploinsufficiency, (B) deletion intolerance scores, (C) duplication intolerance scores, and (D) mean probabilities of conserved targeting (PCT) than non-survivors. (E) PCT score distributions of all gene–miRNA interactions involving human orthologs of survivors (red) and non-survivors (orange) (two-sided Kolmogorov–Smirnov test). Human orthologs of survivors have more miRNA sites conserved between 3′ UTRs of (F) human and chicken orthologs, and (G) human and lizard orthologs than do other ancestral Z genes. Orthologs of survivors are more broadly expressed than the orthologs of non-survivors (H) in a panel of seven adult eastern garter snake tissues, (I) in a panel of eight adult chicken tissues, and (J) in a panel of eight adult human tissues. Orthologs of survivors are more highly expressed than the orthologs of non-survivors (K) in chicken blastocysts, and (L) in human preimplantaion embryos. Orthologs of survivors have reduced d_N/d_S ratios compared to orthologs of non-survivors in alignments between (M) tiger snake and green anole lizard orthologs, (N) chicken and zebra finch orthologs, and (O) human and mouse orthologs.
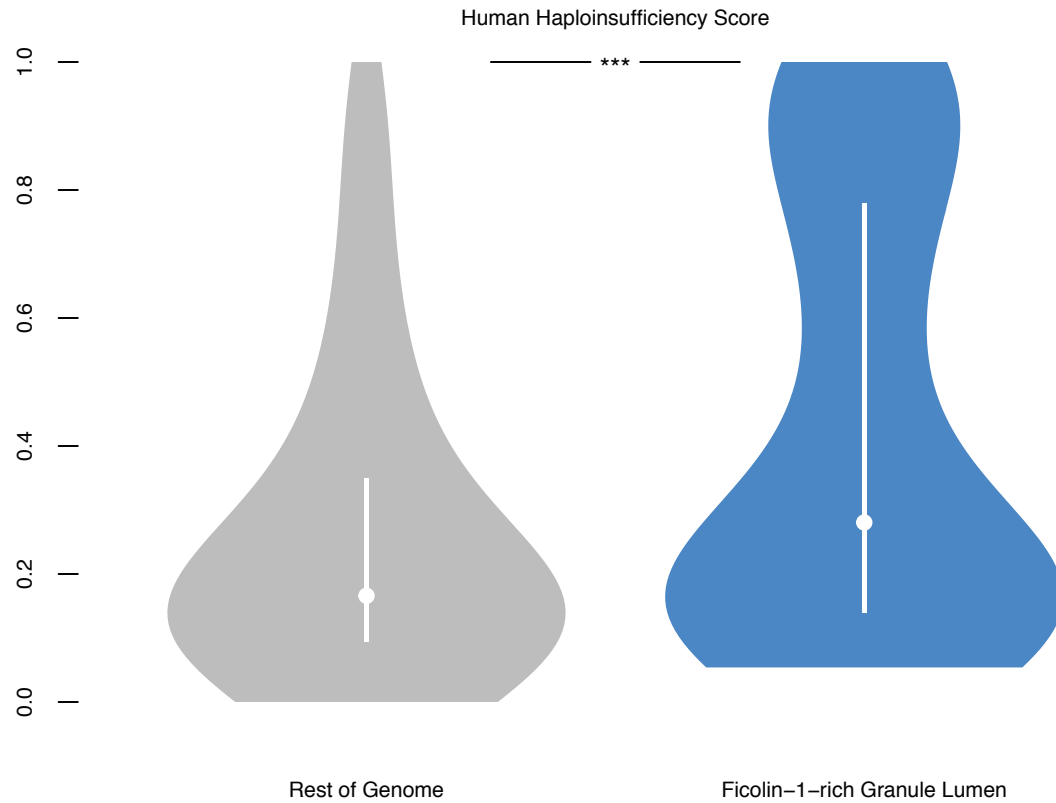
Supplemental Figure S7. Components of ficolin-1-rich granule lumen are dosage-sensitive. Violin plot, with the median (white circle) and interquartile range (white bar) indicated, compares haploinsufficiency of components of ficolin-1-rich granule lumen (blue) to the remainder of genes in the human genome (grey). Components of ficolin-1-rich granule lumen have a greater probability of haploinsufficiency than other human genes (***) P < 0.001, one-tailed Mann–Whitney U test.

Supplemental Figure S8. Dosage sensitivity and broad expression make independent contributions to survival in caenophidian species. A statistical summary of survival factors from 1238 ancestral caenophidian Z genes based on principal component axis one (PC1) and axis two (PC2). Points represent individual genes, colored by their survival fraction from green (no survival) to purple (survival in all possible lineages) (See Supplemental Tables S7 and S18-S21). Arrows show the contribution of each factor to the variation in survival of ancestral genes on sex-specific chromosomes. Dosage sensitivity and breadth of expression make roughly orthogonal contributions, while strength of purifying selection is closely aligned with survival.

Supplemental Figure S9. Dosage sensitivity and broad expression make independent contributions to survival in avian species. A statistical summary of survival factors from 691 ancestral avian Z genes based on principal component axis one (PC1) and axis two (PC2). Points represent individual genes, colored by their survival fraction from yellow(no survival) to pink (survival in all possible lineages) (See Supplemental Tables S7 and S22). Arrows show the contribution of each factor to the variation in survival of ancestral genes on sex-specific chromosomes. Dosage sensitivity and breadth of expression make roughly orthogonal contributions, while strength of purifying selection is closely aligned with survival.
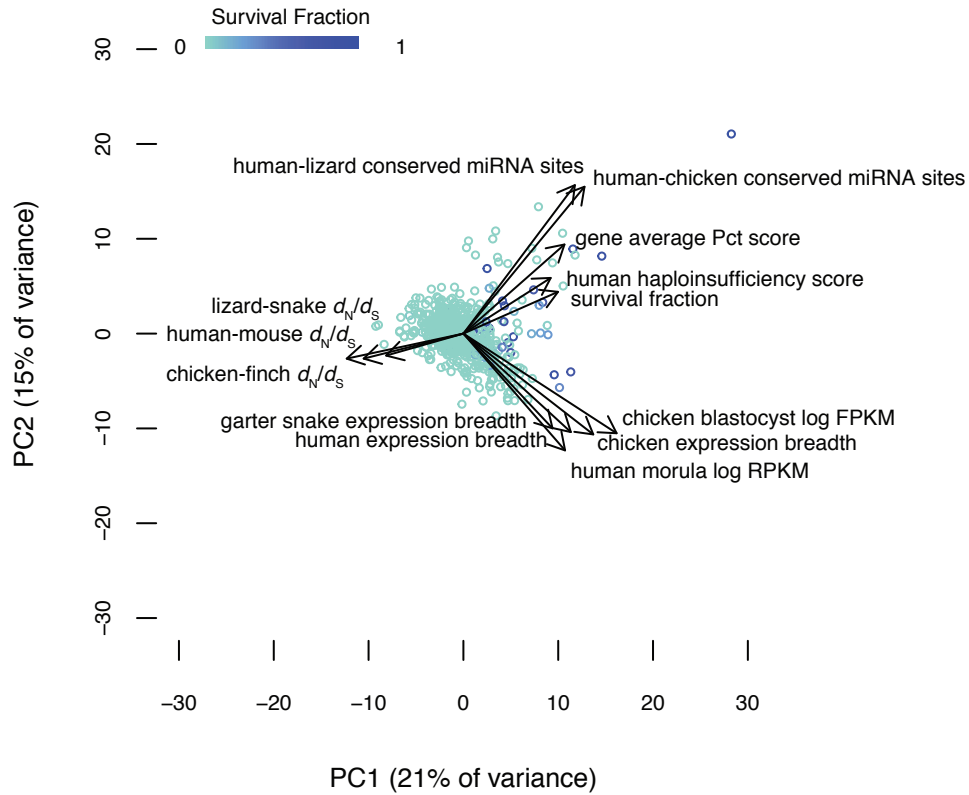
Supplemental Figure S10. Dosage sensitivity and broad expression make independent contributions to survival in therian species. A statistical summary of survival factors from 635 ancestral therian X genes based on principal component axis one (PC1) and axis two (PC2). Points represent individual genes, colored by their survival fraction from cyan(no survival) to blue(survival in all possible lineages) (See Supplemental Tables S7 and S23). Arrows show the contribution of each factor to the variation in survival of ancestral genes on sex-specific chromosomes. Dosage sensitivity and breadth of expression make roughly orthogonal contributions, while strength of purifying selection is closely aligned with survival.